



3 4456 0313417 8

ORNL/TM-11033

# ornl

**OAK RIDGE  
NATIONAL  
LABORATORY**

**MARTIN MARIETTA**

## Component and System Simulation Models for High Flux Isotope Reactor

Ahmet Sozer

OAK RIDGE NATIONAL LABORATORY  
CENTRAL RESEARCH LIBRARY  
CIRCULATION SECTION  
CODE ROOM 125  
**LIBRARY LOAN COPY**  
DO NOT TRANSFER TO ANOTHER PERSON  
If you wish someone else to see this  
report, send in name with report and  
the library will arrange a loan.

OPERATED BY  
MARTIN MARIETTA ENERGY SYSTEMS, INC.  
FOR THE UNITED STATES  
DEPARTMENT OF ENERGY

This report has been reproduced directly from the best available copy.

Available to DOE and DOE contractors from the Office of Scientific and Technical Information, P.O. Box 62, Oak Ridge, TN 37831; prices available from (615) 576-8401, FTS 626-8401.

Available to the public from the National Technical Information Service, U.S. Department of Commerce, 5205 Port Royal Rd., Springfield, VA 22161.

NIS price codes—Printed Copy: A04 Microfiche A01

This report was prepared as an account of work sponsored by an agency of the United States Government. Neither the United States Government nor any agency thereof, nor any of their employees, makes any warranty, express or implied, or assumes any legal liability or responsibility for the accuracy, completeness, or usefulness of any information, apparatus, product, or process disclosed, or represents that its use would not infringe privately owned rights. Reference herein to any specific commercial product, process, or service by trade name, trademark, manufacturer, or otherwise, does not necessarily constitute or imply its endorsement, recommendation, or favoring by the United States Government or any agency thereof. The views and opinions of authors expressed herein do not necessarily state or reflect those of the United States Government or any agency thereof.

ORNL/TM-11033  
Distribution Category UC-505

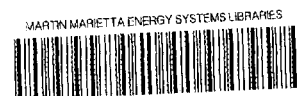
Engineering Technology Division

COMPONENT AND SYSTEM SIMULATION MODELS  
FOR HIGH FLUX ISOTOPE REACTOR

Ahmet Sozer

Publication Date: August 1989

Prepared by the  
OAK RIDGE NATIONAL LABORATORY  
Oak Ridge, Tennessee 37831  
operated by  
MARTIN MARIETTA ENERGY SYSTEMS, INC.  
for the  
U.S. DEPARTMENT OF ENERGY  
under Contract No. DE-AC05-84OR21400



3 4456 0313417 8



## CONTENTS

	<u>Page</u>
ABSTRACT .....	1
1. INTRODUCTION .....	1
2. DESCRIPTION OF THE HFIR SYSTEM .....	3
2.1 HIGH-PRESSURE SYSTEM .....	3
2.2 LOW-PRESSURE SYSTEM .....	3
3. HFIR CORE MODEL .....	5
3.1 POINT KINETICS .....	5
3.2 REACTIVITY .....	9
3.2.1 Core reactivity ( $\rho_b$ ) .....	9
3.2.2 Reactivity from control rods ( $\rho_{cr}$ ) .....	10
3.2.3 Fission product poisoning .....	12
3.2.4 Reactivity from xenon buildup ( $\rho_{Xe}$ ) .....	16
3.2.5 Reactivity from samarium buildup ( $\rho_{Sm}$ ) .....	19
3.3 POWER AND NEUTRON FLUX .....	21
3.4 CORE HEAT TRANSFER.....	21
3.5 DECAY HEAT .....	23
4. HEAT EXCHANGERS .....	24
5. PRIMARY COOLANT HEAD TANK .....	28
5.1 CONSERVATION OF MASS AND ENERGY .....	28
5.2 TANK WATER LEVEL .....	29
6. PUMPS .....	31
7. LETDOWN VALVES .....	33
8. TRANSPORT DELAY (PIPES) .....	34
9. LOOP-PRESSURE-FLOW BALANCE .....	36
9.1 CLOSED-LOOP FLUID SYSTEM .....	36
9.2 NEWTON-RAPHSON METHOD .....	37
10. PRIMARY COOLANT SYSTEM PRESSURE .....	39
11. SUMMARY .....	40
REFERENCES .....	41



## LIST OF FIGURES

<u>Figure No.</u>		<u>Page</u>
1.	HFIR primary coolant system .....	4
2.	Vertical section of HFIR vessel and core. Source: ORNL-3572, Vol. 1B, Revision 2, May 1986 .....	6
3.	Schematic representation of HFIR core .....	7
4.	Control rod positions during a fuel cycle .....	10
5.	Total regulating rod reactivity worth vs position .....	11
6.	Total shim rod reactivity worth (one of four) vs position .....	11
7.	Primary heat exchanger .....	24
8.	Primary coolant head tank .....	28
9.	Characteristic curves for main pressurizer pump ....	31
10.	Characteristic curves for primary coolant pumps ....	32
11.	Schematic diagram of transport delay (pipe) model .....	34
12.	Total available head and fluid system head curves .....	36
13.	Fluid system head with valve throttling vs pump head at different pump speeds .....	37



COMPONENT AND SYSTEM SIMULATION MODELS  
FOR HIGH FLUX ISOTOPE REACTOR

Ahmet Sozer

ABSTRACT

Component models for the High Flux Isotope Reactor (HFIR) have been developed. The models are HFIR core, heat exchangers, pressurizer pumps, circulation pumps, letdown valves, primary head tank, generic transport delay (pipes), system pressure, loop pressure-flow balance, and decay heat. The models were written in FORTRAN and can be run on different computers, including IBM PCs, as they do not use any specific simulation languages such as ACSL or CSMP.

---

1. INTRODUCTION

Component models for the High Flux Isotope Reactor (HFIR) have been developed.\* The models are HFIR-core, heat exchangers, pressurizer pumps, circulation pumps, letdown valves, primary head tank, generic transport delay (pipes), system pressure, loop pressure-flow balance, and decay heat. The models were written in FORTRAN and can be run on different computers, including IBM PCs, as they do not use any specific simulation language such as ACSL or CSMP.

The HFIR core model includes submodels such as six-group point kinetics; heat transfer; control rod worth and position; iodine, xenon, promethium, and samarium concentrations; xenon and samarium poisoning (reactivities); reactivity feedback; and decay heat utilizing time after shutdown vs fraction of operational power.

The heat exchangers were modeled using the effectiveness method, which allows calculation of outlet temperatures of the shell and tube sides using only the overall heat transfer coefficient and inlet temperatures.

---

\*This work was originally done for the application of AI Techniques to the Nuclear Reactors Project. Parts of this work have been incorporated into the LISP machine version of the advanced control design workstation, which is part of the ACTO Program. The models described here are expected to be useful to all ORNL nuclear reactor-related programs.

The pressurizer pump and circulation pumps use manufacturer's pump curves. Letdown valves are equal percentage type and do not include equations for choked flow due mainly to low coolant temperature.

The primary head tank has a cylindrical shape and hemispherical ends. The varying cross section from the bottom to the top of the tank has been accounted for in the calculation of the water level. Energy balance equations were also included for the calculation of water temperature. However, calculation of the water temperature is optional.

The generic transport delay model is used for connecting the components and can be used for calculating transport delay in any of the thermodynamic parameters. It accomplishes this by dividing a connection into a number of equal size nodes specified in the input.

Primary system pressure is calculated as a function of a spring constant, which represents the change in the pressure per gallon of water added or removed from the system, the letdown flow rate, and the pressurizer pump flow rate. (Temperature effect needs to be incorporated in addition to spring constant effect.)

The loop-pressure-flow balance may be modeled using the Newton-Raphson method. For steady state conditions, the Newton-Raphson method calculates primary system flow rate and head developed by circulation pumps until a prespecified convergence criterion is achieved.

The following chapters summarize the basic theories and numerical approaches used to develop the HFIR models.

## 2. DESCRIPTION OF THE HFIR SYSTEM

The primary coolant system is composed of two main subsystems,<sup>1</sup> the high-pressure system with a capacity of 41.62 m<sup>3</sup> (11,000 gal) and the low-pressure system with a capacity of 26.49 m<sup>3</sup> (7,000 gal).

### 2.1 HIGH-PRESSURE SYSTEM

A schematic diagram of the primary coolant system is shown in Fig. 1. The high-pressure system is pressurized and has two main connections to the low-pressure system, pressurizer pump discharge line, and letdown lines. Only three of the four heat exchanger loops are required during normal operation. The four main circulation pumps are driven by ac and dc pony motors under normal operational conditions and by only dc pony motors at low flow conditions. High pressure stainless steel piping connects the reactor vessel with the pumps and heat exchangers. Water passes through a strainer before it enters the top of the reactor vessel through two diametrically opposite 16-in. lines. The outlet from the reactor vessel is a single 18-in. line. There are two main and one emergency pressurizer pumps. The main pressurizer pumps (nine-stage horizontal shaft centrifugal pumps) take water from the primary head tank and discharge into the high-pressure system between the main circulation pumps and the inlet to the reactor. Only one of the main pressurizer pumps is needed under normal operational conditions.

### 2.2 LOW-PRESSURE SYSTEM

The low-pressure (primary cleanup) system is separated from the high-pressure system by the letdown valves and pressurizer pumps. It contains deaerator, pumps, prefilters, demineralizers, afterfilters, primary coolant head tank and interconnecting piping.

The component models included in the HFIR computer model are presented in the following sections.

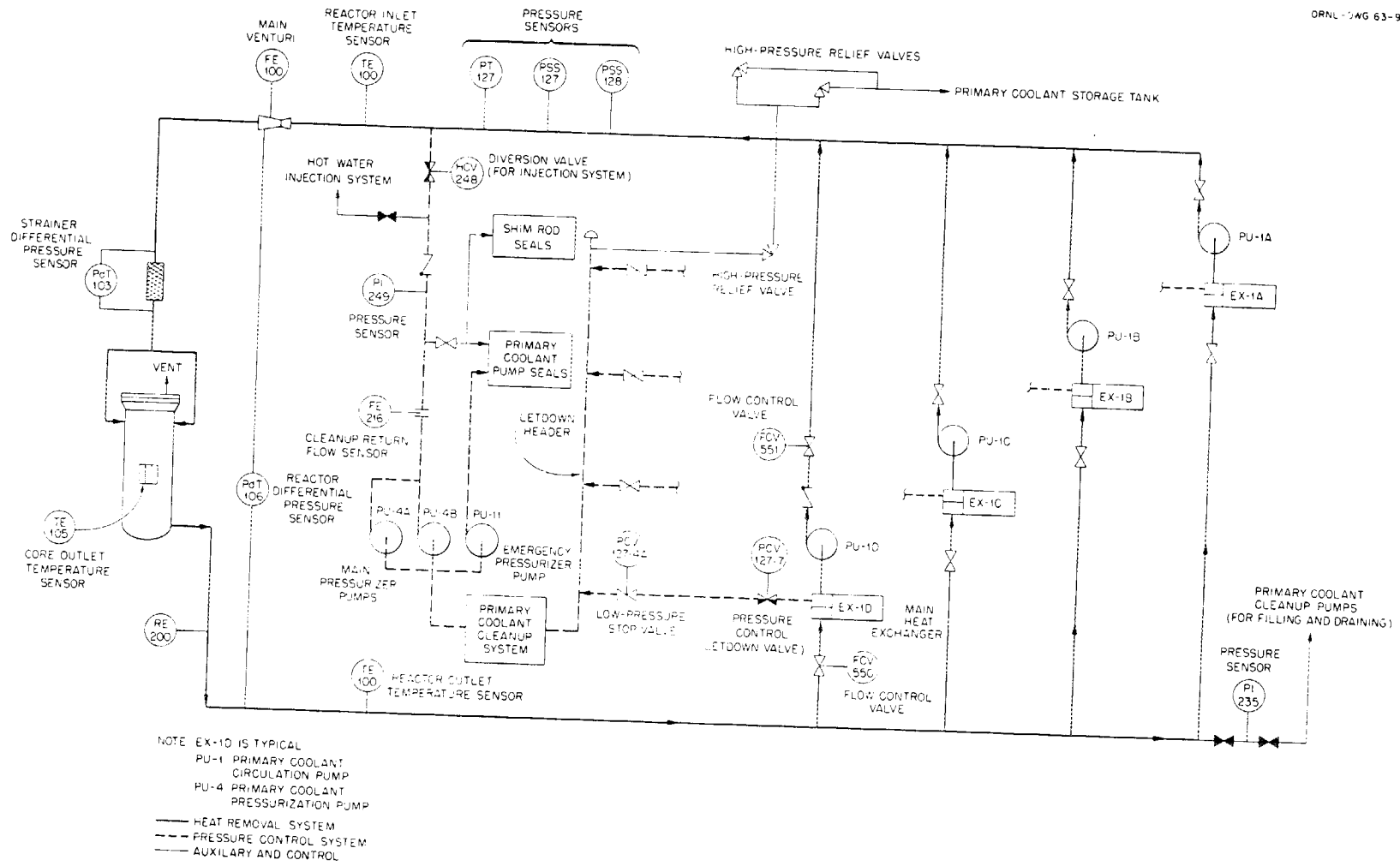


Fig. 1. HFIR primary coolant system.

### 3. HFIR CORE MODEL

A schematic diagram of the vertical cross section of the HFIR vessel is presented in Fig. 2 (reproduced from ref. 1). The HFIR core (Fig. 3) is composed of two cylindrical annular shaped regions. The full length is 60.96 cm (24 in.) and the active fuel length is 50.8 cm (20 in.), with a 43.495-cm-diam (17.124-in.-diam) outer annulus and an 28.575-cm-diam (11.250-in.-diam) inner annulus. The reactor generates about 100 MW(t) during the normal operation, and the average neutron flux at the end of fuel cycle is about  $4.5 \times 10^{14}$  neutrons/cm<sup>2</sup>/s in the fuel region.<sup>1</sup> The control rods are two concentric cylinders located between the outer fuel and the beryllium reflector.

The following sections present point kinetics, reactivity, xenon poisoning, samarium poisoning, control rod worth, neutron flux, decay heat, and heat transfer equations implemented into a subroutine named HFIR01.FOR.

#### 3.1 POINT KINETICS

Six-group point kinetics equations with the prompt jump approximation have been incorporated into the model. The point kinetics equations are

$$\frac{dP}{dt} = \frac{\rho - \beta_T}{\Lambda} P + \sum_i^6 \lambda_i C_i \quad (1)$$

$$\frac{dC_i}{dt} = \frac{\beta_i}{\Lambda} P - \lambda_i C_i, \text{ and} \quad (2)$$

$$\beta_T = \sum_{i=1}^6 \beta_i, \quad (3)$$

where

- P = nuclear power (fission),
- C = neutron precursor concentration,
- $\rho$  = reactivity,
- $\Lambda$  = generation time (s),
- $\beta_i$  = fractional yield of precursor group i,
- $\lambda_i$  = decay constant of precursor group i (s<sup>-1</sup>).

The values of  $\lambda_i$ ,  $\beta_i$ , and  $\beta_T$  were taken from ref. 2 and are shown in Table 1.

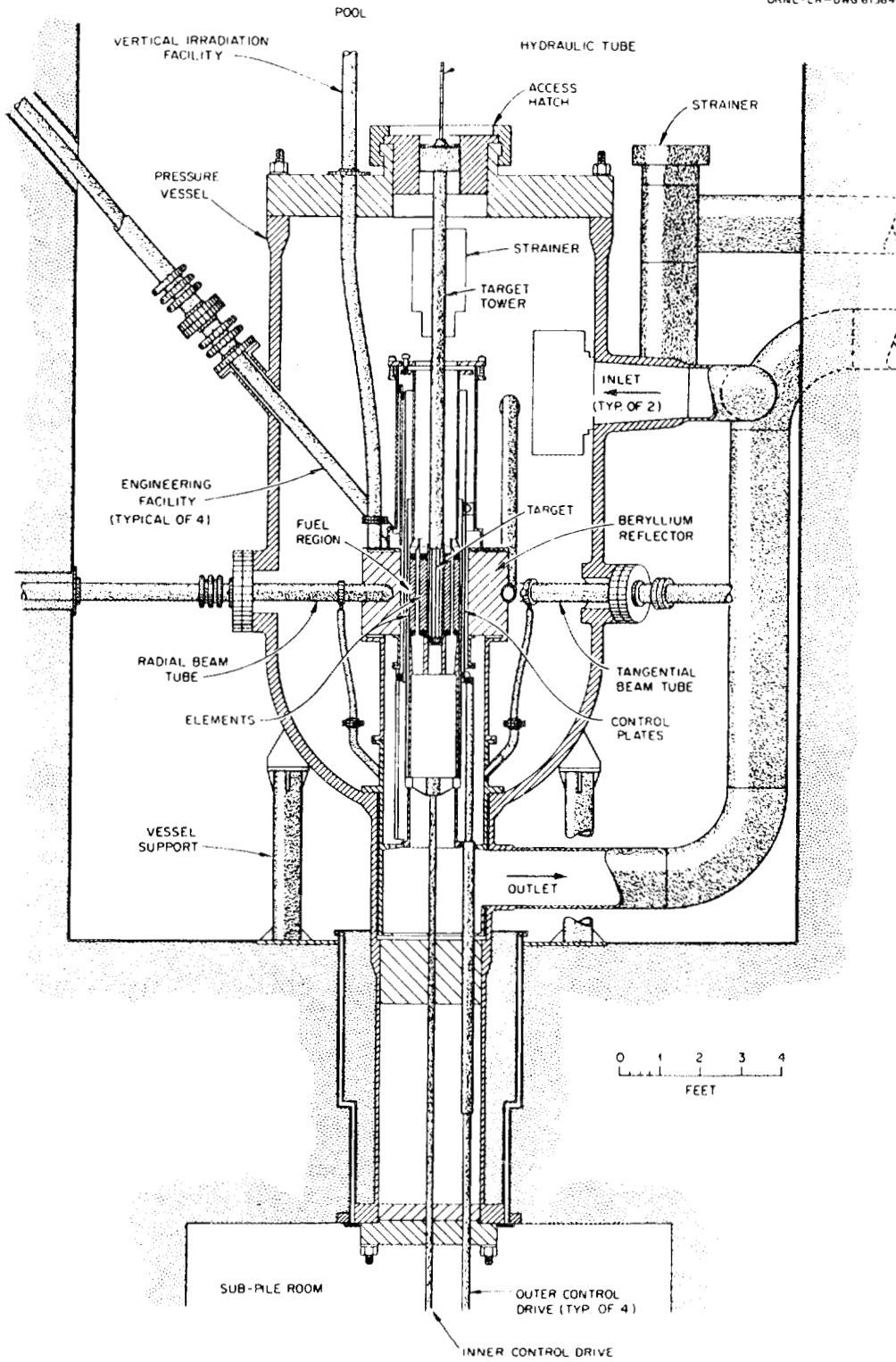


Fig. 2. Vertical section of HFIR vessel and core. Source: ORNL-3572, Vol. 1B, Revision 2, May 1968.

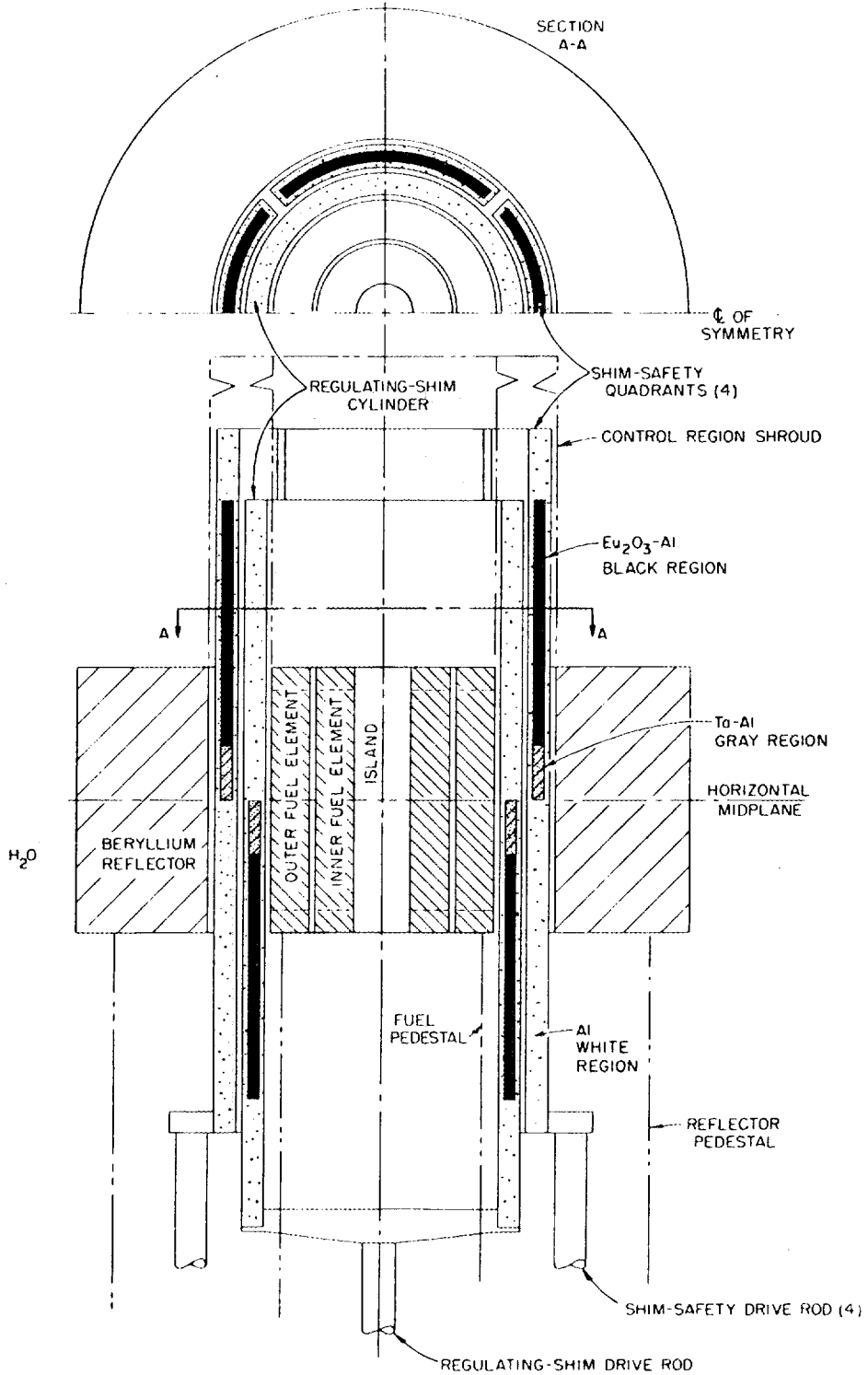


Fig. 3. Schematic representation of HFIR core.

Table 1. Fractional yield and decay constants used in point kinetics equations

$i$	$\beta_i$	$\lambda_i$
1	0.000295	3.01
2	0.000809	1.14
3	0.002767	0.301
4	0.001367	0.111
5	0.001531	0.0305
6	0.000229	0.0124

$$\beta_T = \sum_{i=1}^6 \beta_i = 0.006998$$

Source: D. W. Burke, memorandum, March 6, 1985.

The prompt jump approximation is obtained by setting  $dP/dt$  equal to zero in Eq. (1), which yields the following equation for the calculation of neutron power:<sup>3</sup>

$$P = \frac{\Lambda}{\beta_T - \rho} \sum_{i=1}^6 \lambda_i C_i . \quad (4)$$

Then the solution to the precursor concentration equation (2) is

$$C_i = \frac{\beta_i}{\Lambda \lambda_i} P(1 - e^{-\lambda_i t}) + C_{i0} e^{-\lambda_i t} , \quad (5)$$

where

$C_{i0}$  = initial concentration of precursor group  $i$  and  
 $i = 1, 2, \dots, 6,$

and the initial precursor concentrations are calculated assuming that the reactor is operating at steady state; that is,

$$dC_i/dt = 0,$$

$$C_{i0} = P_0 \frac{\beta_i}{\Lambda \lambda_i} .$$

Equations (4) and (5) are normalized by dividing these equations with the initial power,  $P_0$ ; therefore, the left hand side of Eq. (4) represents power fraction with respect to initial power in the HFIR01.FOR subroutine.

### 3.2 REACTIVITY

The overall reactivity is calculated from the following equation:

$$\rho = \rho_b + \rho_{cr} + \alpha_f (T_f - T_{fr}) + \alpha_w (T_w - T_{wr}) + \rho_{xe} + \rho_{sm} \quad (6)$$

where

- $\rho_b$  = reactivity of isolated core (decreases as burnup continues);
- $\rho_{cr}$  = reactivity of control rods;
- $\rho_{xe}$  = reactivity from xenon buildup;
- $\rho_{sm}$  = reactivity from samarium buildup;
- $\alpha_f$  = fuel temperature coefficient of reactivity;
- $\alpha_w$  = moderator temperature coefficient of reactivity;
- $T_f$  = fuel temperature, °C (°F);
- $T_{fr}$  = reference fuel temperature, °C (°F);
- $T_w$  = moderator temperature, °C (°F);
- $T_{wr}$  = reference moderator temperature, °C (°F).

Fuel and moderator coefficients of reactivity taken from ref. 4 are

Moderator temperature °C (°F)	Fuel coefficient ( $\alpha_w$ )	Moderator coefficient ( $\alpha_f$ )
20.0 (68.0)	$- 1.0 \times 10^{-5}$	$- 5.8 \times 10^{-5}$
68.3 (155.0)	$- 1.6 \times 10^{-5}$	$- 8.7 \times 10^{-5}$
>132.2 (>270.0)		$- 9.7 \times 10^{-5}$

#### 3.2.1 Core reactivity ( $\rho_b$ )

The time-dependent reactivity of isolated core  $\rho_b$  is calculated from curve A of Fig. 7.3.5, ref. 1, for normal steady state operation at 100 MW(t) for a 15-d cycle. The values of  $k_{eff}$  are presented in Table 2. The value of  $\rho_b$  decreases as burnup continues. No burnup model is included in the subroutine HFIR01.FOR; therefore,  $\rho_b$  is an input parameter.

Table 2. Normal steady state operation at 100 MW(t)

Time (d)	$k_{eff}$
0.000	1.09905
0.286	1.07619
0.476	1.06714
0.667	1.06000
1.000	1.05429
1.190	1.05200
1.667	1.04952
8.381	1.02714
12.000	1.01333
14.857	1.00000

Source: Curve A, Fig. 7.3.5, ORNL-3572, vol. 1A, Revision 2, May 1968.

### 3.2.2 Reactivity of control rods ( $\rho_{cr}$ )

The two kinds of control rods are shim and regulating. As shown in Fig. 4, the rods consist of three sections: high neutron-absorbing (black), moderately neutron-absorbing (gray), and comparatively poor neutron-absorbing (white). The rod worth of the control rods is presented in Figs. 5 and 6 and by the following equations taken from ref. 5. (Originals of Figs. 5 and 6 and the equations are not in SI units.)

$$\rho_{cr} = \rho_{reg} + 4.0 \times \rho_{shim}$$

ORNL-LR-DWG 46129AR

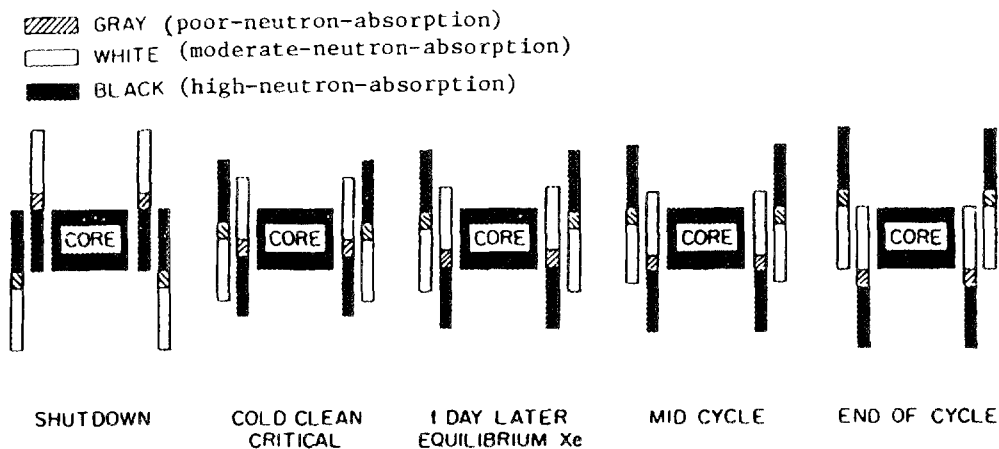


Fig. 4. Control rod positions during a fuel cycle.

ORNL-DWG 89-4303 ETD

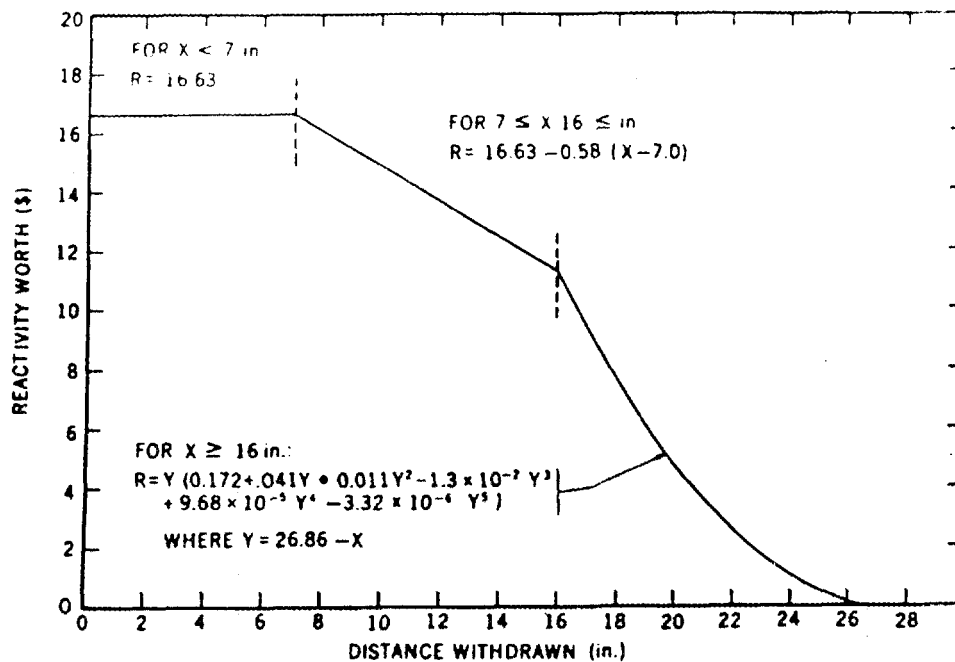


Fig. 5. Total regulating rod reactivity worth vs position.

ORNL-DWG 89-4304 ETD

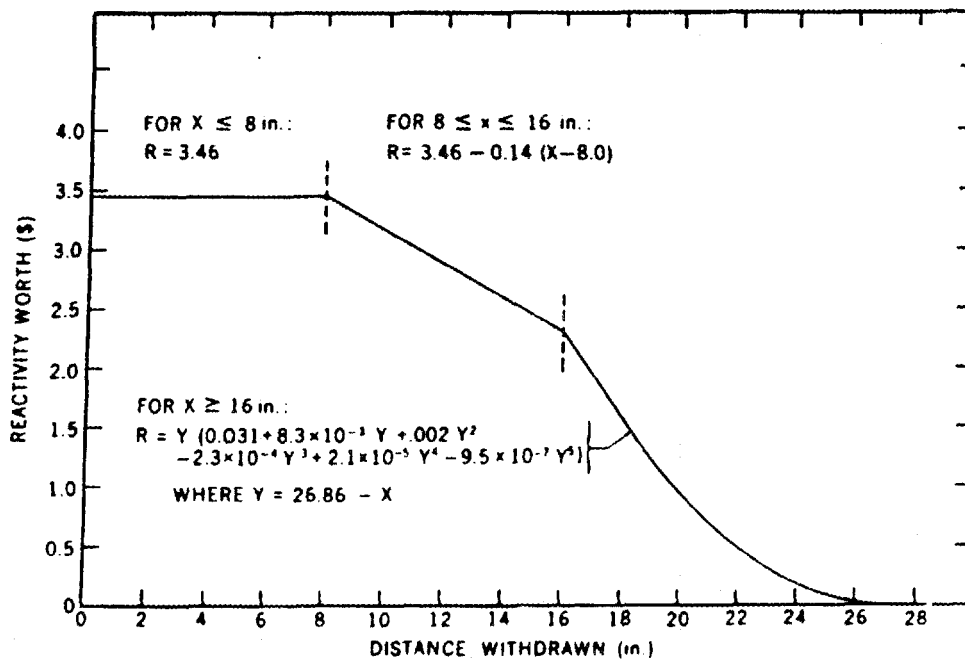


Fig. 6. Total shim rod reactivity worth (one of four) vs position.

Reactivity worth of regulating rods ( $\rho$ )	Distance withdrawn (x)
$\rho_{\text{reg}}/\beta_T = 16.63$	$x < 17.78 \text{ cm (7 in)}$
$\rho_{\text{reg}}/\beta_T = 16.63 - 0.58 (x - 7.0)$	$17.78 \text{ cm} \leq x \leq 40.64 \text{ cm (16 in)}$
$\rho_{\text{reg}}/\beta_T = Y(0.172 + 0.041 Y +$ $+ 0.011 Y^2 - 1.3 \times 10^{-3} Y^3$ $+ 9.68 \times 10^{-5} Y^4 - 3.32 \times 10^{-6} Y^5)$	$x \geq 40.64 \text{ cm (16 in)}$

where  $Y = 26.86 - x$ .

Reactivity worth of shim rods ( $\rho$ ) (one of four)	Distance withdrawn (x)
$\rho_{\text{shim}}/\beta_T = 3.46$	$x \leq 20.32 \text{ cm (8 in)}$
$\rho_{\text{shim}}/\beta_T = 3.46 - 0.14 (x - 8.0)$	$20.32 \text{ cm} \leq x \leq 40.64 \text{ cm (16 in)}$
$\rho_{\text{shim}}/\beta_T = Y(0.031 + 8.3 \times 10^{-3} Y$ $+ 0.002 Y^2 - 2.3 \times 10^{-4} Y^3$ $+ 2.1 \times 10^{-5} Y^4 - 9.5 \times 10^{-7} Y^5)$	$x \geq 40.64 \text{ cm (16 in)}$

where  $Y = 26.86 - X$ .

Given rod position, reactivity of control rods is calculated in the RODWOR.FOR routine. Given a core reactivity, a control rod position that makes the overall reactivity zero is calculated in RODPOS.FOR.

### 3.2.3 Fission product poisoning

Fission product poisoning is a concern in thermal reactors (ref. 3). Xenon and samarium have large absorption cross sections, and their concentration depends on the present and recent past operating neutron power level. There are many other fission products; however, because of their far smaller cross sections, they are not depleted by neutron capture. These fission products, called permanent poisons, tend to accumulate in a reactor core. Their combined effective absorption cross section is about 50 b per fission.<sup>3,6</sup> They are accounted for in

criticality and burnup calculations.<sup>3</sup> The HFIR core model neglects the effects of permanent poisons on reactivity. The reactivity from xenon ( $^{135}\text{Xe}$ ) and samarium ( $^{149}\text{Sm}$ ) is incorporated into the HFIR model as described in Sects. 3.2.4 and 3.2.5.

Following the argument on fission product poisoning in refs. 3 and 6, negative reactivity generated by xenon and samarium may be computed as follows: The reactivity change from a critical reactor in which poison concentration is zero is given by

$$\Delta\rho = \frac{k' - k}{k'}$$

where

$$k = npf\epsilon P_{fnl} P_{tnl} .$$

$$\Delta\rho = \frac{f' - f}{f'} + \frac{P'_{tnl} + P_{tnl}}{P'_{tnl}}$$

where

$$P_{tnl} = \frac{1}{1 + L^2 B_g^2} .$$

$$\Delta\rho \approx \frac{f' - f}{f'}$$

where

$$L^2 B_g^2 \ll 1 .$$

$k$  = multiplication factor without poison,

$k'$  = multiplication factor with poison,

$f$  = thermal utilization factor,

$f'$  = thermal utilization factor with poison,

$\nu$  = average number of neutrons released per fission,

$n$  = number of fission neutrons produced per absorption in the fuel,

$p$  = resonance escape probability,

$\epsilon$  = fast fission factor.

$P_{fnl}$  is the nonleakage probability of fast neutrons and not expected to

vary much. (At neutron energies above 1.0 eV, the absorption cross sections of  $^{135}\text{Xe}$  and  $^{149}\text{Sm}$  drop rapidly.)  $P_{\text{tnl}}$  is the nonleakage probability of thermal neutrons. ( $L^2B_g^2$  is small because leakage is small.) The thermal utilization factor for a homogeneous reactor is defined by

$$f = \frac{\Sigma_a^f}{\Sigma_a^f + \Sigma_a^m} = \frac{\Sigma_a^f}{\Sigma_a}$$

without poisons and

$$f' = \frac{\Sigma_a^f}{\Sigma_a^f + \Sigma_a^m + \Sigma_a^p} = \frac{\Sigma_a^f}{\Sigma_a + \Sigma_a^p}$$

with poisons

where

$$\Sigma_a = \Sigma_a^f + \Sigma_a^m,$$

$\Sigma_a^f$  = macroscopic absorption cross section of fuel,

$\Sigma_a^m$  = macroscopic absorption cross section of moderator,

$\Sigma_a^p$  = macroscopic absorption cross section of poison.

Thus,

$$\Delta\rho = - \frac{\Sigma_a^p}{\Sigma_a} . \quad (7)$$

For a critical reactor,  $k = \eta p \epsilon P_{\text{fnl}} P_{\text{tnl}} = 1$ . The following three approximations allow calculation of  $\Delta\rho$  in terms of  $\nu$ ,  $\Sigma_a^f$  and  $\Sigma_a^p$ :

$$1) \quad \eta = \nu \sigma_f^f / \sigma_a^f, \quad \eta \approx \nu,$$

$$2) \quad p \epsilon \approx 1, \text{ and}$$

$$3) \quad f = \frac{\Sigma_a^f}{\Sigma_a} \approx 1/\nu$$

where

$\sigma_a^f$  = absorption cross section of fuel and

$\sigma_f^f$  = fission cross section of fuel.

Then negative reactivity introduced by a poison can be calculated from the following equation:

$$\Delta\rho = -\frac{1}{\nu} \frac{\Sigma_a^P}{\Sigma_a^f} \quad (9)$$

HFIR is a heterogeneous reactor. Thermal utilization factor for heterogeneous reactors is

$$f = \frac{\Sigma_a^f}{\Sigma_a^f + \Sigma_a^m \frac{V_m}{V_f} \frac{\phi_m}{\phi_f} + \Sigma_a^{cr} \frac{V_{cr}}{V_f} \frac{\phi_{cr}}{\phi_f} + \Sigma_a^c \frac{V_c}{V_f} \frac{\phi_c}{\phi_f} + \Sigma_a^r \frac{V_r}{V_f} \frac{\phi_r}{\phi_f}}$$

$$= \frac{\Sigma_a^f}{\Sigma_a^f} \text{ without poison ,}$$

$$f = \frac{\Sigma_a^f}{\Sigma_a^f + \Sigma_a^P} \text{ with poison}$$

where

$\Sigma_a^{cr}$ ,  $\Sigma_a^c$ ,  $\Sigma_a^r$  = macroscopic absorption cross sections of control rods, clad, and reflector

$V_m$ ,  $V_f$ ,  $V_{cr}$ ,  $V_c$ ,  $V_r$  = volumes of moderator, fuel, control rods, clad, and reflector

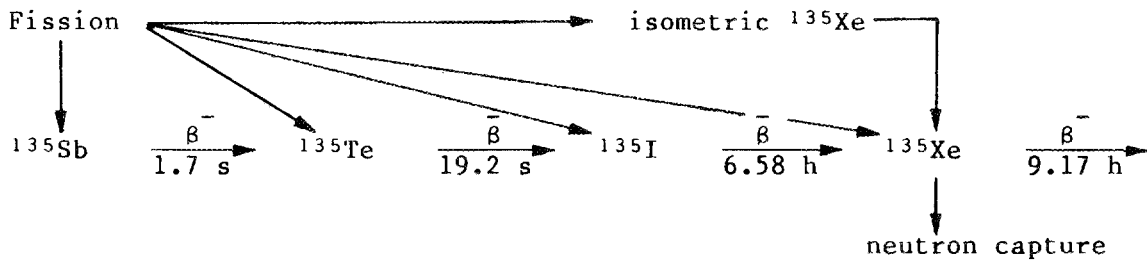
$\phi_f$ ,  $\phi_m$ ,  $\phi_{cr}$ ,  $\phi_c$ ,  $\phi_r$  = neutron flux in fuel, moderator, control rods, clad, and reflector.

With poison, neutron flux distribution will be altered. Application of

the above method with the assumption that flux distribution is not altered is expected to yield approximate values for poison reactivities.

### 3.2.4 Reactivity from xenon buildup ( $\rho_{xe}$ )

Core composition affects neutron flux and power distribution. Because Xenon-135 is a fission product and has a very large thermal neutron absorption cross section, small amounts of  $^{135}\text{Xe}$  may significantly affect core  $k_{\text{eff}}$  by absorbing neutrons needed to sustain the chain reaction. The life chain of  $^{135}\text{Xe}$  is<sup>3</sup>



Because of the relatively small decay constants of the fission products  $^{135}\text{Sb}$  and  $^{135}\text{Te}$ ,  $^{135}\text{Xe}$  concentration can be represented by the following equations:

$$\text{iodine: } \frac{\partial I}{\partial t} = \gamma_I \Sigma_f \phi - \lambda_I I \quad \text{and} \quad (10)$$

$$\text{xenon: } \frac{\partial X}{\partial t} = \gamma_X \Sigma_f \phi + \lambda_I I - \lambda_X X - \sigma_a^X \phi X . \quad (11)$$

The steady state values obtained by setting  $\partial I/\partial t = 0$  and  $\partial X/\partial t = 0$  are

$$I = \frac{\gamma_I \Sigma_f \phi}{\lambda_I} \quad (12)$$

and

$$X = \frac{\Sigma_f \phi (\gamma_X + \gamma_I)}{\lambda_X + \sigma_a^X \phi} . \quad (13)$$

The solutions to Eqs. (10) and (11) are

$$I = \frac{\gamma_I \Sigma_f \phi}{\lambda_I} \left( 1 - e^{-\lambda_I t} \right) + I_0 e^{-\lambda_I t} , \quad (14)$$

$$\begin{aligned}
X = & \frac{(\gamma_x + \gamma_I)\Sigma_f\phi}{\lambda_x + \sigma_a^x\phi} \left[ 1 - e^{-(\lambda_x + \sigma_a^x\phi)t} \right] \\
& + \frac{\gamma_I\Sigma_f\phi}{\lambda_x - \lambda_I + \sigma_a^x\phi} \left[ e^{-(\lambda_x + \sigma_a^x\phi)t} - e^{-\lambda_I t} \right] \\
& + \frac{\lambda_I I_0}{\lambda_x - \lambda_I + \sigma_a^x\phi} \left[ e^{-\lambda_I t} - e^{-(\lambda_x + \sigma_a^x\phi)t} \right] + X_0 e^{-(\lambda_x + \sigma_a^x\phi)t}, \quad (15)
\end{aligned}$$

where

I = iodine concentration,

X = xenon concentration,

I<sub>0</sub> = initial iodine concentration,

X<sub>0</sub> = initial xenon concentration,

γ<sub>I</sub> = yield fraction of <sup>135</sup>I (0.06386),

γ<sub>x</sub> = yield fraction of <sup>135</sup>Xe (0.00228),

λ<sub>I</sub> = decay constant of <sup>135</sup>I (2.875 × 10<sup>-5</sup> s<sup>-1</sup>),

λ<sub>x</sub> = decay constant of <sup>135</sup>Xe (2.0917 × 10<sup>-5</sup> s<sup>-1</sup>),

φ = neutron flux (neutron/cm<sup>2</sup> s),

σ<sub>a</sub><sup>x</sup> = absorption cross section of <sup>135</sup>Xe (2.7 × 10<sup>-18</sup> cm<sup>2</sup>),

Σ<sub>f</sub> = macroscopic fission cross section of <sup>235</sup>U.

The macroscopic fission cross section, Σ<sub>f</sub>, for the HFIR core is calculated as follows:

$$\Sigma_f = N_u \sigma_f,$$

where

density of U<sub>3</sub>O<sub>8</sub> = 8.2 gm cm<sup>-3</sup>,

N<sub>u</sub> = number density of <sup>235</sup>U (1.778 × 10<sup>22</sup> cm<sup>-3</sup>),

σ<sub>f</sub> = fission cross section of <sup>235</sup>U (280 × 10<sup>-24</sup> cm<sup>2</sup>).

The above values result in Σ<sub>f</sub> = 4.97788 cm<sup>-1</sup>. All of the constants were taken from ref. 3.

Xenon reactivity can be estimated using Eq. (7):

$$\rho_{Xe} = - \frac{\Sigma_a^x}{\Sigma_a} \quad (16)$$

where

$$\Sigma_a^x = X \sigma_a^x ,$$

$\Sigma_a$  = total absorption cross section .

After  $\Sigma_f$  is factored out in Eq. (15), Xe concentration (X) is substituted into Eq. (16). Then the reactivity from Xe buildup is calculated with the help of Eq. (8):

$$\begin{aligned} \rho_{Xe} = & - \frac{\sigma_a^x}{\nu} \left\{ \frac{(\gamma_x + \gamma_I)\phi}{\lambda_x + \sigma_a^x \phi} \left[ 1.0 - e^{-(\lambda_x + \sigma_a^x \phi)t} \right] \right. \\ & + \frac{\gamma_I \phi}{\lambda_x - \lambda_I + \sigma_a^x \phi} \left[ e^{-(\lambda_x + \sigma_a^x \phi)t} - e^{-\lambda_I t} \right] \\ & + \frac{-\lambda_I I_0}{\Sigma_f (\lambda_x - \lambda_I + \sigma_a^x \phi)} \left[ e^{-\lambda_I t} - e^{-(\lambda_x + \sigma_a^x \phi)t} \right] \\ & \left. + \frac{X_0}{\Sigma_f} e^{-(\lambda_x + \sigma_a^x \phi)t} \right\} . \quad (17) \end{aligned}$$

The steady state value of Xe reactivity may be calculated from

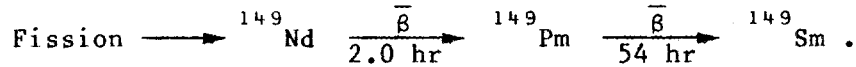
$$\rho_{Xe} = - \frac{\sigma_a^x \phi (\gamma_x + \gamma_I)}{\nu (\lambda_x + \sigma_a^x \phi)} \quad (18)$$

where  $\nu = 2.432$  neutrons/fission is used.

Equations (14), (15), and (17) are general solutions and can be applied to startup of a clean core, xenon transients following power level changes, and reactor shutdown.

### 3.2.5 Reactivity from samarium buildup ( $\rho_{sm}$ )

Samarium is another fission product that has a large absorption cross section ( $\sigma_a^s = 58,500$  b) similar to that of  $^{135}\text{Xe}$ . However, the concentration of  $^{149}\text{Sm}$  can be reduced only by neutron capture because  $^{149}\text{Sm}$  is stable. The life chain is<sup>3</sup>



Because of its relatively short lifetime,  $^{149}\text{Nd}$  can be neglected and we can assume that fission yields  $^{149}\text{Pm}$  directly.

The conservation equations are

$$\text{Promethium: } \frac{\partial \text{Pm}}{\partial t} = \gamma_p \Sigma_f \phi - \lambda_p \text{Pm} , \text{ and} \quad (19)$$

$$\text{Samarium: } \frac{\partial \text{Sm}}{\partial t} = \lambda_p \text{Pm} - \sigma_a^s \phi \text{Sm} . \quad (20)$$

The steady state values, which can be calculated by setting  $\partial \text{Pm}/\partial t = 0.0$  and  $\partial \text{Sm}/\partial t = 0.0$ , are

$$\text{Pm} = \frac{\gamma_p \Sigma_f \phi}{\lambda_p}$$

and

$$\text{Sm} = \frac{\gamma_p \Sigma_f \phi}{\sigma_a^s} ,$$

where

Pm = promethium concentration,

Sm = samarium concentration,

$\gamma_p$  = promethium yield fraction (0.0113),

$\lambda_p$  = decay constant of promethium ( $3.55556 \times 10^{-6} \text{ s}^{-1}$ ),

$\sigma_a^s$  = absorption cross section of samarium ( $5.85 \times 10^{-20} \text{ cm}^2$ ).

The values for the constants were taken from ref. 3.

The solution to Eq. (19) is

$$P_m = \frac{\gamma_p \Sigma_f \phi}{\lambda_p} \left( 1 - e^{-\lambda_p t} \right) + P_{m_0} e^{-\lambda_p t} . \quad (21)$$

Then, Eq. (21) is substituted into Eq. (20) and the solution for Sm concentration is

$$S_m = \frac{\gamma_p \Sigma_f}{\sigma_a^s} \left( 1 - e^{-\sigma_a^s \phi t} \right) + \frac{\gamma_p \Sigma_f \phi - \lambda_p P_{m_0}}{\sigma_a^s \phi - \lambda_p} \left( e^{-\sigma_a^s \phi t} - e^{-\lambda_p t} \right) + S_{m_0} e^{-\sigma_a^s \phi t} . \quad (22)$$

where

$P_{m_0}$  = initial concentration of promethium and

$S_{m_0}$  = initial concentration of samarium.

The corresponding reactivity can be calculated using the same approach used for calculating Xe-reactivity:

$$\rho_{Sm} = - \frac{\Sigma_a^s}{\Sigma_a} = - \frac{S_m \sigma_a^s}{\Sigma_a}$$

$$\frac{\Sigma_f}{\Sigma_a} \approx \frac{1}{\nu} .$$

Then reactivity from samarium buildup is

$$\rho_{Sm} = - \frac{\sigma_a^s}{\nu} \left[ \frac{\gamma_p}{\sigma_a^s} \left( 1 - e^{-\sigma_a^s \phi t} \right) + \frac{\gamma_p \phi - \lambda_p P_{m_0} / \Sigma_f}{\sigma_a^s \phi - \lambda_p} \left( e^{-\sigma_a^s \phi t} - e^{-\lambda_p t} \right) + S_{m_0} / \Sigma_f e^{-\sigma_a^s \phi t} \right] . \quad (23)$$

The steady state value of  $\rho_{Sm}$  reactivity is

$$\rho_{Sm} = -\frac{\gamma_p}{\nu} . \quad (24)$$

### 3.3 POWER AND NEUTRON FLUX

Reactor power is calculated from Eq. (4) as indicated in the point kinetics section. The relationship between power and neutron flux can then be used to calculate a neutron flux as follows:

$$P = \phi w_f \Sigma_f V \quad (25)$$

and

$$\phi = P/w_f \Sigma_f V , \quad (26)$$

where

- $\phi$  = neutron flux,
- $P$  = power,
- $w_f$  = amount of energy generated per fission reaction,
- $V$  = fuel volume,
- $P$  = 100 MW(t),
- $w_f$  = 192.9 Mev/fission (ref. 3),
- $V$  = 1455.47 cm<sup>3</sup>,
- $\Sigma_f$  = 4.97788 cm<sup>-1</sup>.

These values give a neutron flux equal to  $4.4659 \times 10^{14}$  cm<sup>-2</sup> s<sup>-1</sup>, which is close to the magnitude of the neutron flux at the end of the fuel cycle in the fuel region. The macroscopic cross section  $\Sigma_f$  will change as the number density of fissionable material changes. The model uses a constant value.

### 3.4 CORE HEAT TRANSFER

The core is represented by fuel and coolant nodes, as it is in ref. 7.

The conservation of energy equation for the coolant node is

$$M_w C_{pw} \frac{dT_w}{dt} = bP - W_w C_{pw} (T_{wo} - T_{wi}) + UA (T_f - T_w) , \quad (27)$$

and the conservation of energy equation for the fuel node is

$$M_f C_{pf} \frac{dT_f}{dt} = aP - UA (T_f - T_w), \quad (28)$$

where

- A = heat transfer area, m<sup>2</sup> (ft<sup>2</sup>);
- U = overall heat transfer coefficient, W/m<sup>2</sup>K (Btu/ft<sup>2</sup> h°F);
- M<sub>w</sub> = mass of water in the coolant node, kg (lb<sub>m</sub>);
- M<sub>f</sub> = mass of fuel, kg (lb<sub>m</sub>);
- C<sub>pw</sub> = specific heat of water, J/kg K (Btu/lb<sub>m</sub>°F);
- C<sub>pf</sub> = specific heat of fuel node, J/kg K (Btu/lb<sub>m</sub>°F);
- W<sub>w</sub> = flow rate of coolant, kg/s (lb<sub>m</sub>/s);
- T<sub>w</sub> = average temperature of water, °C (°F) = 0.5 × (T<sub>wi</sub> + T<sub>wo</sub>), ;
- T<sub>wi</sub> = core inlet temperature, °C (°F),
- T<sub>wo</sub> = core outlet temperature, °C (°F),
- T<sub>f</sub> = average temperature of fuel node, °C (°F),
- P = power, W (Btu/s);
- a = fraction of total power generated in fuel;
- b = fraction of power generated in the coolant by neutron slow-down and γ rays.

A semi-implicit approach has been used to solve Eqs. (27) and (28). The temperatures on the right-hand side of the equations are represented by the average values of the temperatures at two different time steps (n and n+1); that is,

$$dT_f = T_f^{n+1} - T_f^n, \quad T_f = (T_f^{n+1} + T_f^n)/2,$$

$$dT_w = T_w^{n+1} - T_w^n, \quad \text{and } T_w = (T_w^{n+1} + T_w^n)/2.$$

The final equations for average fuel and coolant temperatures are

$$T_f^{n+1} = \frac{1}{\frac{M_f C_{pf}}{\Delta t} + \frac{UA}{2}} \left[ \left( \frac{M_f C_{pf}}{\Delta t} - \frac{UA}{2} \right) T_f^n + \frac{UA}{2} T_w^{n+1} + \frac{UA}{2} T_w^n + a P^{n+1} \right] \quad (29)$$

$$T_w^{n+1} = \frac{1}{D - \frac{0.25 U^2}{E}} \left[ \left( B + \frac{0.25 U^2}{E} \right) T_w^n + \left( \frac{0.5 UA}{E} F + 0.5 UA \right) T_f^n + A + \frac{0.5 UA}{E} a P^{n+1} \right] \quad (30)$$

where

$$A = bP^{n+1} + \frac{M_w C_{pw}}{\tau} T_{wi}^{n+1},$$

$$B = \frac{C_{pw}}{\Delta t} - \frac{C_{pw}}{2\tau} - \frac{UA}{2},$$

$$D = \frac{M_w C_{pw}}{\Delta t} + \left( \frac{M_w C_{pw}}{\tau} + UA \right) / 2,$$

$$E = \frac{M_f C_f}{\Delta t} + \frac{UA}{2},$$

$$F = \frac{M_f C_{pf}}{\Delta t} - \frac{UA}{2},$$

$$\tau = M_w / W_w \quad (\text{time constant}).$$

### 3.5 DECAY HEAT

Reactor power does not sharply decrease to zero when a reactor is shut down. Through neutron,  $\beta$ , and  $\gamma$  decay, fission products continue to decay at decreasing rates after shutdown. Because of these decay processes, the reactor continues to generate power. The amount of power generated depends on the power level before shutdown, the time period of that level, and elapsed time after shutdown.<sup>8</sup>

Decay power is represented in subroutine DCHEAT.FOR as time after shutdown vs fraction of operational power.<sup>9</sup> Because irradiation time in HFIR is much shorter than in PWRs and BWRs, the current decay heat curve is conservative and needs to be replaced by a decay heat curve representative of HFIR.

## 4. HEAT EXCHANGERS

The primary heat exchangers are parallel-counter-flow (shell and U-tube type) and mounted vertically (Fig. 7). Each heat exchanger is designed to remove 34-1/3 MW(t) from the primary coolant loop. Only three heat exchangers are required for full-power operation.

The effectiveness method combined with the lumped parameter approach has been used in modeling heat exchangers. The shell and tube sides are represented by single nodes. The advantages of the effectiveness method over the logarithmic mean temperature difference (LMTD) method are

1. The effectiveness method allows calculation of the net heat transfer rate without knowledge of outlet temperatures.

2. It does not present a see-saw effect when a step change is made in the inlet temperatures, and it allows outlet temperatures to change in the direction consistent with the underlying physics. (Use of LMTD with single nodes causes outlet temperature to drop when a step increase is made in the inlet temperatures or vice-versa.<sup>10</sup>)

ORNL-DWG 89-4305 ETD

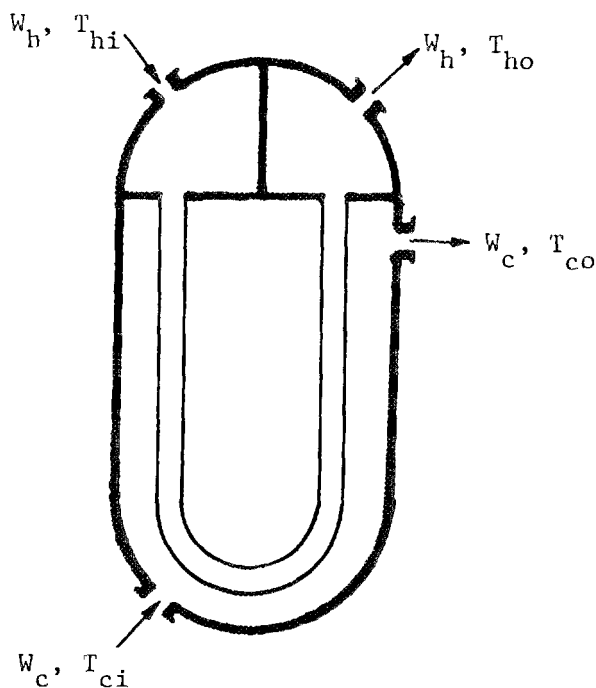


Fig. 7. Primary heat exchanger.

Effectiveness is defined by

$$E = \frac{C_h (T_{hi} - T_{ho})}{C_{\min} (T_{hi} - T_{ci})} = \frac{C_c (T_{co} - T_{ci})}{C_{\min} (T_{hi} - T_{ci})}$$

$$C_{\min} = \min (C_h, C_c) \quad (31)$$

where

$$C_h = W_h C_{ph} = \text{flow rate} * \text{specific heat of the hot side, W/K (Btu/°F s)};$$

$$C_c = W_c C_{pc} = \text{flow rate} * \text{specific heat of the cold side, W/K (Btu/°F s)};$$

$$C_{\min} = \text{minimum of } C_h \text{ and } C_c, \text{ W/K (Btu/°F s)};$$

$$T_{hi} = \text{hot side inlet temperature, °C (°F)};$$

$$T_{ho} = \text{hot side outlet temperature, °C (°F)};$$

$$T_{ci} = \text{cold side inlet temperature, °C (°F)};$$

$$T_{co} = \text{cold side outlet temperature, °C (°F)}.$$

The rate of heat transfer from the tube side to the shell side ( $\dot{Q}$ ) is determined from

$$\dot{Q} = E C_{\min} (T_{hi} - T_{ci}) . \quad (32)$$

Independent of outlet temperatures, the effectiveness for a parallel-counter-current (shell-and-tube) heat exchanger is<sup>11</sup>

$$E = \frac{2}{\frac{1 + C_{\min}}{C_{\max}} + \left[ 1 + \left( \frac{C_{\min}}{C_{\max}} \right)^2 \right]^{0.5} \left( \frac{1 + e^{-\Gamma}}{1 - e^{-\Gamma}} \right)} \quad (33)$$

where

$$\Gamma = \frac{UA}{C_{\min}} [1 + (C_{\min}/C_{\max})^2]^{0.5} , \quad (34)$$

$$C_{\max} = \max (C_h, C_c),$$

$$UA = \text{overall heat transfer coefficient times heat transfer surface area, W/K (Btu/°F s)}.$$

The overall heat transfer coefficient times the total surface area (UA) is calculated from the steady state values of the parameters. Equation (30) is substituted into Eq. (33) and solved for UA. The resulting equation is

$$UA = - \frac{C_{\min}}{b} \ln [(c - 1)/(c + 1)] \quad (35)$$

where

$$\begin{aligned} b &= [1 + (C_{\min}/C_{\max})^2]^{0.5} \\ c &= [2 - E(1 + C_{\min}/C_{\max})]/(Eb) \\ E &= C_h (T_{hi} - T_{ho})/[C_{\min}(T_{hi} - T_{ci})] . \end{aligned}$$

The UA term is assumed to remain constant during transients, and effectiveness is calculated from Eq. (33) for every time step (n). (An improvement can be made by allowing UA to be flow-dependent.) The total heat transfer rate is calculated from Eq. (32) and used in the following equations for calculation of outlet temperatures:

$$\frac{dT_{ho}}{dt} = \frac{w_h}{M_h} (T_{hi} - T_{ho}) - \frac{\dot{Q}}{M_h C_{ph}} , \text{ and} \quad (36)$$

$$\frac{dT_{co}}{dt} = \frac{w_c}{M_c} (T_{ci} - T_{co}) + \frac{\dot{Q}}{M_c C_{pc}} . \quad (37)$$

The total mass terms  $M_h$  and  $M_c$  include both water and metal masses and are described by

$$M_h = V_h \rho_h + \frac{C_{pt}}{C_{ph}} \frac{M_{\text{tube}}}{2} , \text{ and} \quad (38)$$

$$M_c = V_c \rho_c + \frac{C_{ps}}{C_{pc}} M_{\text{shell}} + \frac{C_{pt}}{C_{pc}} \frac{M_{\text{tube}}}{2} . \quad (39)$$

The explicit approach has been used to solve Eqs. (36) and (37).

Definitions of the terms used in the equations are

$$\begin{aligned} V_h, V_c &= \text{water volumes of hot and cold sides, m}^3 \text{ (ft}^3\text{)}; \\ \rho_h, \rho_c &= \text{water density of hot and cold sides, kg/m}^3 \text{ (lb}_m\text{/ft}^3\text{)}; \\ C_{pt}, C_{ps} &= \text{specific heat of tube and shell metal, J/kg K} \\ &\quad \text{(Btu/}^\circ\text{F lb}_m\text{)}; \end{aligned}$$

$M_{\text{tube}}$  = total tube metal mass, kg ( $lb_m$ );  
 $M_{\text{shell}}$  = total shell metal mass, kg ( $lb_m$ ).

The tube side is the hot side and the shell side is the cold side. The heat exchanger subroutine is HEATEX.FOR.

## 5. PRIMARY COOLANT HEAD TANK

The primary coolant head tank provides the necessary suction head for the pressurizer pumps. It receives letdown return flow, primary head tank makeup flow; and small flows from pump seals, reactor tank top vent, pressurizer pump, and pressure relief. It is positioned horizontally as shown in Fig. 8.

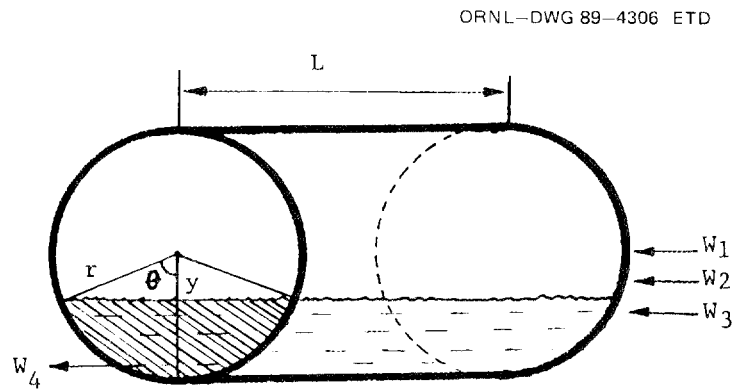


Fig. 8. Primary coolant head tank.

## 5.1 CONSERVATION OF MASS AND ENERGY

The primary coolant head tank model includes mass and optional energy balances for calculating water level and water temperature. The pressure in the tank is atmospheric. The lumped parameter approach has been used. Water in the tank is assumed to be well mixed and is represented by a single node.

Conservation of water mass:

$$\frac{dM}{dt} = W_1 + W_2 + W_3 - W_4, \quad (40)$$

where

- $M$  = water mass in the tank, kg ( $lb_m$ );
- $W_1$  = make up flow rate, kg/s ( $lb_m/s$ );
- $W_2$  = letdown flow rate, kg/s ( $lb_m/s$ );
- $W_3$  = combined flow rate of small flows, kg/s ( $lb_m/s$ );
- $W_4$  = pressurizer pump flow, kg/s ( $lb_m/s$ ).

Calculation of water temperature is optional. If it is not selected in the input, only water level is calculated. Conservation of energy:

$$\frac{d}{dt} (MC_p T) = W_1 C_{p1} T_1 + W_2 C_{p2} T_2 + W_3 C_{p3} T_3 - W_4 C_{p4} T_4 . \quad (41)$$

The left-hand side of the equation is expanded as follows:

$$\frac{d}{dt} (MC_p T) = C_p T \frac{dM}{dt} + C_p M \frac{dT}{dt} , \quad (42)$$

where T's and Cp's are temperatures and specific heats and are associated with water in the tank and the flows. The value of dM/dt is substituted from the conservation of mass equation. Temperature, T, on the right-hand side of the equation is defined as an average of its values in two consecutive time steps (n and n + 1) as follows:

$$dT = T^{n+1} - T^n \text{ and } T = (T^{n+1} + T^n)/2 .$$

The final equation for the water temperature is

$$T^{n+1} = \frac{1 - \frac{\Delta t}{2M} (W_1 + W_2 + W_3)^{n+1}}{1 + \frac{\Delta t}{2M} (W_1 + W_2 + W_3)^{n+1}} T^n + \frac{\frac{\Delta t}{MC_p} (C_{p1} W_1 T_1 + C_{p2} W_2 T_2 + C_{p3} W_3 T_3)^{n+1}}{1 + \frac{\Delta t}{2M} (W_1 + W_2 + W_3)^{n+1}} , \quad (43)$$

where

$$M = (M^n + M^{n+1})/2 .$$

## 5.2 TANK WATER LEVEL

The tank is a horizontal cylinder; hence, its cross sectional area changes from zero to a max value (2rL) at the midplane. The water level is calculated from water inventory in the tank in the following manner. The area of shaded segment of the circle in Fig. 8 is

$$A = \frac{1}{2} r^2 (\theta - \sin\theta) , \quad (44)$$

and the volume of water is

$$V = AL ,$$

where

$L$  = length of the tank, m (ft);

$r$  = radius of the tank, m (ft);

$\theta$  = angle .

Then

$$\theta = \sin\theta + \frac{2V}{Lr^2} , \quad (45)$$

only  $\theta$  is not known in the equation. This equation is solved using a trial-and-error method in the primary head tank subroutine. The relationship between  $\theta$  and  $y$  (the distance between the water surface and the center of the tank cross sectional area) is

$$y = r \cos(\theta/2) . \quad (46)$$

Now water level can be calculated as a function of  $y$ :

if  $0^\circ \leq \theta \leq 180^\circ$  , water level =  $r - y$ ;

if  $180 \leq \theta \leq 360$  , water level =  $r + y$  .

The control valve for the tank maintains a water level corresponding to 75% capacity [7.1 m<sup>3</sup> (1875 gal)]. If level drops low enough corresponding to 25% capacity [2.4 m<sup>3</sup> (625 gal)], the main pressurizer pumps will shut off and the emergency pressurizer pump will automatically start. Neither of these two control features are included in the tank model. The length and the diameter of the tank are 3.56 m (11.667 ft) and 1.98 m (6.5 ft) respectively. The primary head tank subroutine is PHEADT.FOR.

6. PUMPS

Pumps have been modeled using total pump head vs flow rate curves, which were taken from ref. 1. The curves implemented as tables into the model use linear interpolation between two data points. Pressurizer pump curves are represented in Fig. 9 and primary coolant pump curves in Fig. 10. Pump curves have been extrapolated down to zero pump head.

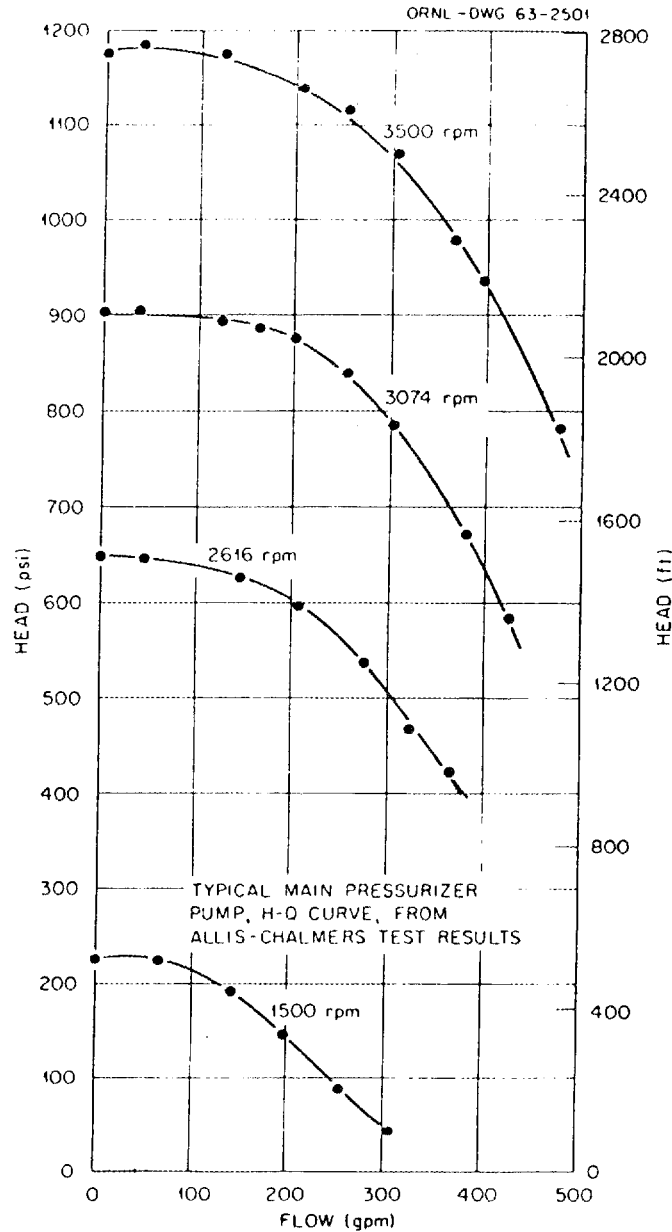


Fig. 9. Characteristic curves for main pressurizer pump.

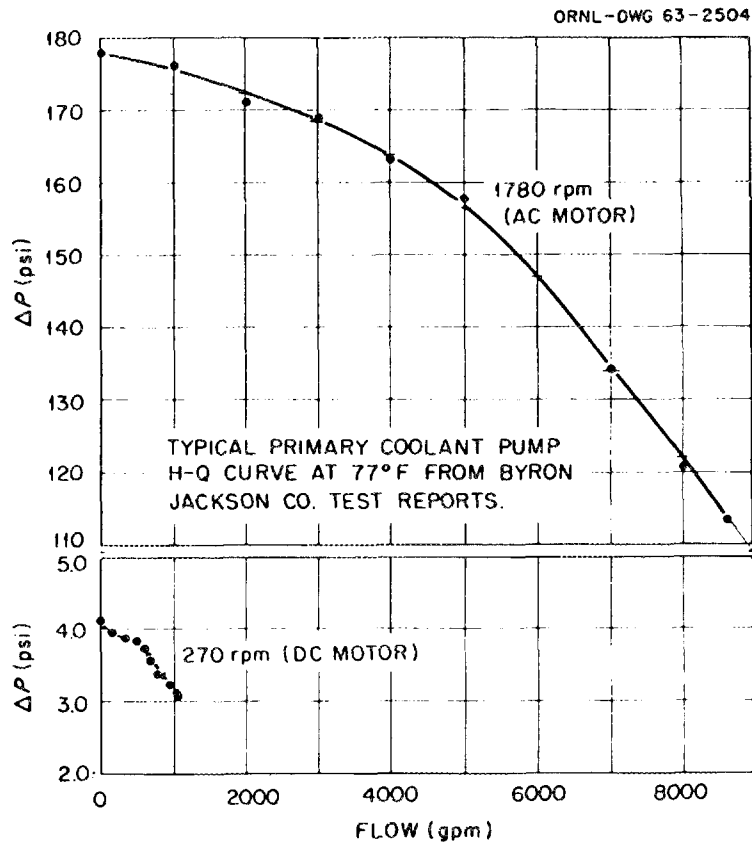


Fig. 10. Characteristic curves for primary coolant pumps.

The flow coastdown curves for primary and secondary coolant pumps are provided in Ref. 12 but currently are not included in the model. The subroutines are PUMPCR.FOR and PUMPPR.FOR.

## 7. LETDOWN VALVES

The letdown valves have equal percentage characteristics and a maximum  $C_v$  equal to 8.7 (ref. 13). Flow coefficient,  $C_v$ , is a function of valve opening and is calculated as<sup>10</sup>

$$C_v = Y^3 (C_v)_{\max} , \quad (47)$$

where  $Y$  = fractional valve opening. Flow rate through the valve is

$$Q = C_v \sqrt{\Delta P 62.4/\rho} , \quad (48)$$

where

$Q$  = volumetric flow rate,  $m^3/s$  (gpm);

$C_v$  = flow coefficient,  $m^3/s Pa^{0.5}$  (gpm/psi<sup>0.5</sup>);

$\Delta P$  = pressure drop through valve, Pa (psi);

$\rho$  = water density,  $kg/m^3$  ( $lb_m/ft^3$ ).

The letdown valve subroutine is VALVE.FOR.

## 8. TRANSPORT DELAY (PIPES)

Pipes are represented by a transport delay model. Because the model is generic, it can be used for delays in transportation of temperature, enthalpy, or any other quantity moving at the speed of the fluid in a pipe. The subroutine is called TDELAY.FOR, which can keep track of delays in different connections simultaneously. The following assumptions are made: (1) the fluid is incompressible, and (2) the flow is plug flow. Heat losses and the heat capacity of pipe walls are presently neglected; however, they can be incorporated if needed. A pipe is divided into a number of equal size nodes (determined in the input), and the cross sectional area is assumed to be uniform. A simple schematic diagram of transport delay in a pipe is shown in Fig. 11. The pipe is filled from one end and emptied from the other. The shaded area represents the incoming slug at time step  $n+1$ . Outlet conditions will change depending on the incoming velocity of the fluid at time step  $(n+1)$ ; that is, as the number of nodes has been filled with the new values of transported variables. Two variables being transported in this model are  $T$  (temperature) and  $W$  (representing any other quantity such as flow rate).

The distance ( $X$ ) traveled inside the pipe by the incoming fluid at time step  $(n+1)$  is

$$x^{n+1} = V^{n+1} \Delta t + x_0^n, \quad (49)$$

where

$x_0$  = distance less than node length and traveled by the fluid in the previous time step,  $m$  (ft);

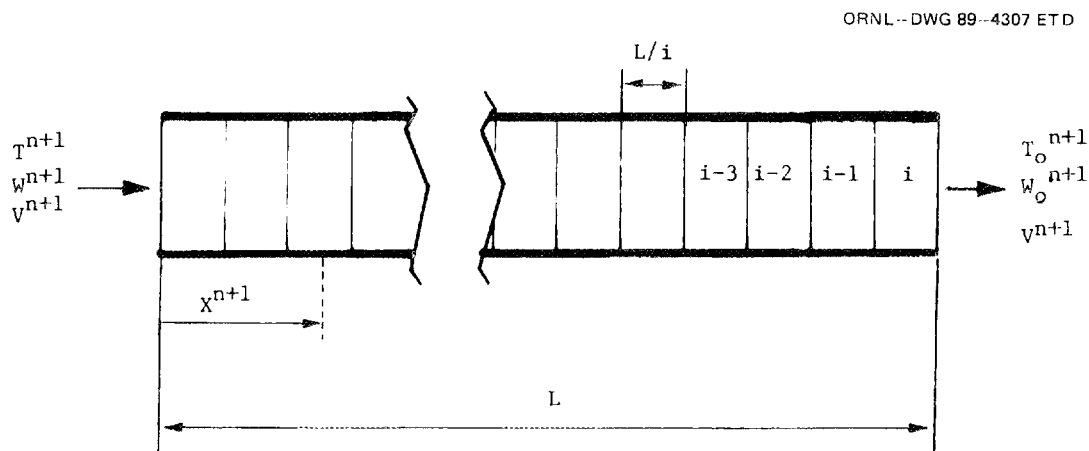


Fig. 11. Schematic diagram of transport delay (pipe) model.

$V$  = velocity of the incoming fluid,  $m$  (ft/s);

$\Delta t$  = time step (s).

Total number of nodes displaced by the incoming fluid of time step (n+1) is

$$m^{n+1} = \text{Integer} (x^{n+1}/\Delta L) . \quad (50)$$

The distance between the front of a slug and the boundary of the most recent node passed by the slug is

$$x_0^{n+1} = x^{n+1} - m \Delta L , \quad (51)$$

where  $\Delta L$  = node length  $m$  (ft).

The outlet conditions are calculated as follows:

for  $m = i$  (52)

$$T_o^{n+1} = [T(i) + T(i-1) + \dots + T(i-m+1)]/m$$

$$w_o^{n+1} = [w(i) + w(i-1) + \dots + w(i-m+1)]/m ,$$

for  $i > m \geq 1$  (53)

$$T_o^{n+1} = [T(i) + T(i-1) + \dots + T(i-m)]/m$$

$$w_o^{n+1} = [w(i) + w(i-1) + \dots + w(i-m)]/m ,$$

and for  $m = 0$  (54)

$$T_o^{n+1} = T_o^n$$

$$w_o^{n+1} = w_o^n ,$$

where  $i$  = maximum number of nodes.

The transport delay subroutine is TDELAY.FOR.

## 9. LOOP-PRESSURE-FLOW BALANCE

A summary of total system head and total pump head balance is provided in Sect. 9.1. The Newton-Raphson method is suitable for computing equilibrium flow rate in a loop and is summarized in Sect. 9.2.

### 9.1 CLOSED-LOOP FLUID SYSTEM

For a closed-loop fluid system, the total head generated by circulation pumps must be equal to the combination of all losses during steady state operation. Otherwise, fluid will accelerate or decelerate until the combination of all losses becomes equal to the total pump head. A fluid system curve is shown in Fig. 12.

The losses that may be accounted for include friction, form, kinetic, and elevation. In a closed-loop fluid system with constant density fluid, elevation losses will be zero.

Total fluid system head can be altered by throttling or bypassing the valve. Both of these processes can be used to increase or decrease friction and form losses, thus changing the equilibrium point represented by the cross section of the curves in Fig. 13. Pump head curves at different speeds are also shown. Pump flow rate and head at different speeds may be calculated by use of the affinity laws<sup>14</sup> (i.e.,  $Q_2^2/Q_1^2 = H_2/H_1$  and  $Q_2/N_2 = Q_1/N_1$ , where  $Q$  = flow rate,  $H$  = pump head, and  $N$  = pump speed). Total pump head may also be altered by changing the impeller diameter or connecting pumps in series (pressure additive). Pumps connected in parallel (flow additive) will develop the same head at their equivalent flow rates for the developed head.

ORNL-DWG 89-4308 ETD

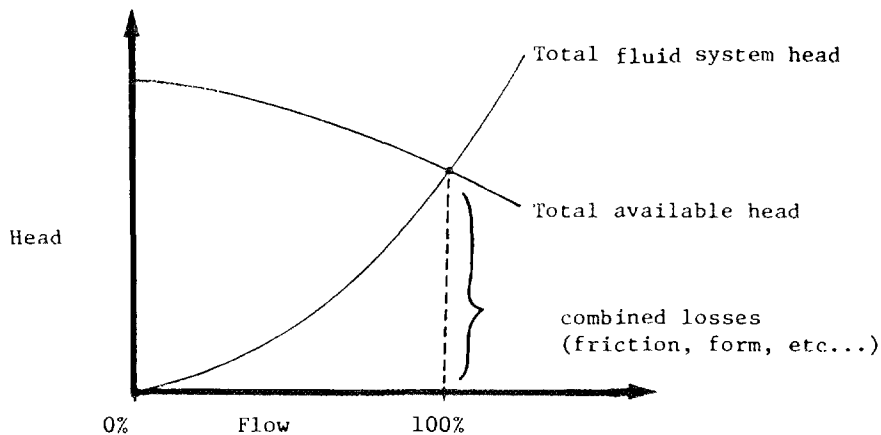


Fig. 12. Total available head and fluid system head curves.

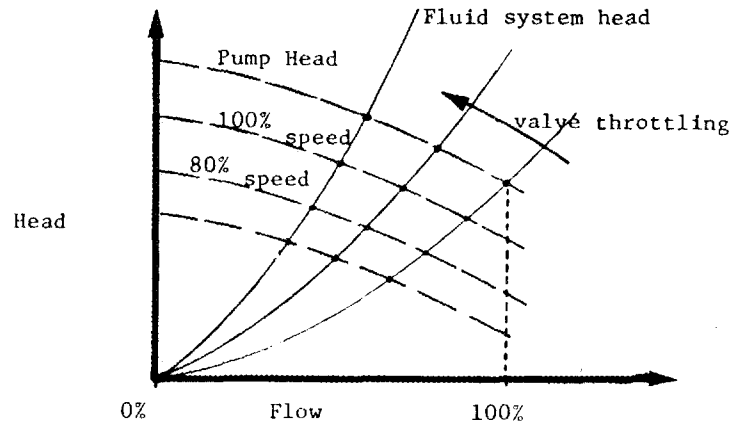


Fig. 13. Fluid system head with valve throttling vs pump head at different pump speeds.

## 9.2 NEWTON-RAPHSON METHOD

The Newton-Raphson method is an iterative method, and the accuracy of a solution depends on a tolerance factor. This method is suitable for calculating pressure-flow balance (ref. 14) as illustrated by the following example for a constant-speed pump in a loop.

Total pump head is defined by  $H(Q)$  and total system head (combined losses) by  $K Q^2$ . The letter  $K$  represents a constant including friction and form loss factors, and the letter  $Q$  represents flow rate. In this example,  $K$  is assumed to be independent of  $Q$ . We seek a solution of  $Q$  such that pump head balances combined losses in the system as follows:

$$F(Q) = H(Q) - K Q^2 = 0 . \quad (55)$$

$F(Q)$  is expanded into Taylor series. Only the first two terms are included.

$$F(Q) = F(Q_0) + \left. \frac{dF(Q)}{dQ} \right|_{Q_0} dQ , \quad (56)$$

where  $Q_0$  is the first estimate.

$F(Q)$  is set equal to zero and solved for a better estimate of  $Q$ . In terms of  $n$  number of iterations, the new estimate is

$$Q^{n+1} = Q^n - \frac{F(Q^n)}{\left( \frac{dF}{dQ} \right)_{Q^n}} , \quad (57)$$

where

$$F(Q^n) = H(Q^n) - K (Q^n)^2, \text{ and}$$

$$\left(\frac{dF}{dQ}\right)_{Q^n} = \left[\frac{dH(Q)}{dQ}\right]_{Q^n} - 2 K Q^n. \quad (58)$$

The term  $dH(Q)/dQ$  at  $Q^n$  is calculated from the pump curves because it represents the slope of the pump head at  $Q^n$ . Iteration continues until  $|Q^{n+1} - Q^n| < \epsilon$ , where  $\epsilon$  represents the tolerance factor.

## 10. PRIMARY COOLANT SYSTEM PRESSURE

The high-pressure primary system is filled with liquid water. Imbalances between letdown flow and pressurizer pump flow cause system pressure to change. Hydraulic testing of HFIR coolant system was performed,<sup>12</sup> and the volumetric expansion coefficient for the high-pressure system (also referred to as "spring constant") was determined to be

$$K = 35.93 \text{ MPa/m}^3 = 19.7 \text{ psi/gal}$$

from these tests. (This value has previously been used by refs. 2 and 13.)

Primary coolant system pressure is calculated from

$$\frac{dP}{dt} = K (Q_{pr} - Q_{ld})/60.0 , \quad (59)$$

where

$P$  = pressure, Pa (psi);

$t$  = time (s);

$Q_{pr}$  = pressurizer pump flow rate, m<sup>3</sup>/s (gpm);

$Q_{ld}$  = letdown flow rate, m<sup>3</sup>/s (gpm).

The primary coolant system pressure subroutine is PPRESS.FOR. Because temperature changes can have a big effect on system pressure, an accurate model should include the effect of temperature on system pressure.

## 11. SUMMARY

The following individual models have been developed for HFIR: HFIR core, heat exchangers, pumps, primary head tank, transport delay, and system pressure. The Newton-Raphson method is recommended for calculating loop-pressure-flow balance. This work was performed for the Application of AI Techniques to Nuclear Reactors Project.

## REFERENCES

1. *The High Flux Isotope Reactor, A Functional Description*, ORNL-3572 vols. 1A and 1B, (Rev. 2) May 1968.
2. D. W. Burke, "Analog Computer Analysis of Loss of Pressure Accidents in the HFIR," memorandum to M. W. Kohring, ORNL, March 6, 1985.
3. J. L. Duderstadt and L. J. Hamilton, *Nuclear Reactor Analysis*, John Wiley & Sons, pp. 567-77, 1976.
4. R. D. Cheverton, D. W. Burke, and T. E. Cole, *HFIR Transients and Reactivity Accountability*, ORNL/TM-1747, January 18, 1967.
5. J. B. Bullock and H. P. Danforth, *Reactor On-Line Computer Control Development at the HFIR, Vol. 1: Objectives, System Design, Operating Experience, and Safety Considerations*, ORNL/TM-3679, October 23, 1972.
6. J. R. Lamarsh, *Introduction to Nuclear Reactor Theory*, Addison-Wesley, pp. 467-477, 1966.
7. R. S. Stone and D. W. Burke, *An Investigation of the Effects of Some Safety System Modifications on the Safety of the HFIR*, ORNL/TM-5738, June 1977.
8. M. M. El-Wakil, *Nuclear Heat Transport*, American Nuclear Society, 1978.
9. Dr. F. E. Haskin, private communication, Subject: "Whole Core Decay Heat Power," Sandia National Laboratories, January 28, 1986.
10. *Modular Modeling System (MMS): A Code for the Dynamic Simulation of Fossil and Nuclear Power Plants, Vol. 1: Theory Manual*, Babcock & Wilcox, March 1985.
11. W. M. Kays and A. L. London, *Compact Heat Exchangers*. The National Press, 1955.
12. G. J. Dixon, internal memorandum, December 18, 1964.
13. S. J. Ball, "Results of Loss of Pressure Accident Study for HFIR," memorandum to N. Hilvety, ORNL, January 12, 1962.
14. N. P. Cheremisinoff, *Fluid Flow, Pumps, Pipes, and Channels*, Ann Arbor Sci. Pub., 1982.



## INTERNAL DISTRIBUTION

- |     |                   |        |                                     |
|-----|-------------------|--------|-------------------------------------|
| 1.  | S. J. Ball        | 22.    | J. A. Mullens                       |
| 2.  | J. C. Cleveland   | 23.    | F. R. Mynatt                        |
| 3.  | J. C. Conklin     | 24.    | P. J. Otaduy                        |
| 4.  | D. H. Cook        | 25.    | J. T. Robinson                      |
| 5.  | B. L. Corbett     | 26.    | A. E. Ruggles                       |
| 6.  | W. G. Craddick    | 27.    | D. B. Simpson                       |
| 7.  | T. L. Dahl        | 28.    | T. Sofu                             |
| 8.  | D. M. Eissenberg  | 29-32. | A. Sozer                            |
| 9.  | M. B. Farrar      | 33.    | R. P. Taleyarkhan                   |
| 10. | G. F. Flanagan    | 34.    | W. E. Thomas                        |
| 11. | E. C. Fox         | 35.    | H. E. Trammell                      |
| 12. | R. M. Harrington  | 36.    | M. W. Wendel                        |
| 13. | R. W. Hobbs       | 37.    | C. D. West                          |
| 14. | S. S. Hurt        | 38.    | T. L. Wilson                        |
| 15. | J. E. Jones, Jr.  | 39.    | ORNL Patent Section                 |
| 16. | L. E. Klobe       | 40-42. | Laboratory Records Department       |
| 17. | T. S. Kress       | 43.    | Laboratory Records (RC)             |
| 18. | A. L. Lotts       | 44-45. | Central Research Library            |
| 19. | A. P. Malinauskas | 46.    | Y-12 Technical Reference<br>Section |
| 20. | D. G. Morris      |        |                                     |
| 21. | D. L. Moses       |        |                                     |

## EXTERNAL DISTRIBUTION

47. Assistant Manager for Energy Research and Development, DOE-ORO, Oak Ridge, Tennessee 37831-2001.
48. Dr. S. H. Bush, Review & Syntheses Associates, 630 Cedar Avenue, Richland, Washington 99352
49. W. C. Gilbert, U.S. Department of Energy, Oak Ridge Operations Office, Oak Ridge, Tennessee 37831
50. Dr. A. N. Goland, Brookhaven National Laboratory, Building 179-A, Upton, New York 11973
51. Dr. J. M. Hendrie, Brookhaven National Laboratory, Building 197-C, Upton, New York 11973
52. E. E. Hoffman, U.S. Department of Energy, Oak Ridge Operations Office, Oak Ridge, Tennessee 37831
53. T. M. Jelinek, U.S. Department of Energy, Oak Ridge Operations Office, Oak Ridge, Tennessee 37831
54. G. R. Irwin, 7306 Edmonston Avenue, College Park, Maryland 20740
- 55-59. C. L. Matthews, U.S. Department of Energy, Oak Ridge Operations Office, Oak Ridge, Tennessee 37831
60. Dr. D. J. Michel, Department of Mechanical Engineering, Naval Post Graduate School, Monterey, California 93940
61. J. D. Rothrock, U.S. Department of Energy, Oak Ridge Operations Office, Oak Ridge, Tennessee 37831
62. Dr. P. G. Shewman, 2477 Lytham Road, Columbus, Ohio 43220

63. L. E. Steele, 7624 Highland Street, Springfield, Virginia 22150
64. A. P. L. Turner, Dominion Engineering, 6862 Elm Street, Suite 460, McLean, Virginia 22101
65. Dr. J. R. Weeks, Brookhaven National Laboratory, Building 703, Upton, New York 11973
- 66-168. Given distribution as shown in DOE/OSTI-4500 under category UC-505 (Mathematics and Computer Sciences)